Techniques for generation of annular surface plasmon polaritons with refractive binary and reflective cylindrical diffraction gratings

B.A. Knyazev[a)], Yu.Yu. Choporova, V.V. Gerasimov, O.E. Kameshkov,
I.Sh. Khasanov, S.E. Krasnopevtsev, A.K. Nikitin, N.D. Osintseva[b)], V.S. Pavelyev

Novosibirsk State University, 630090, Russia, Novosibirsk Region, Novosibirsk, 1, Pirogova str.
[a)] ba_knyazev@phys.nsu.ru
[b)] Corresponding author: natalyaosintseva@gmail.com

Abstract. The propagation length of surface plasmon polaritons (SPPs) increases with increasing wavelength, which makes it possible to use radiation from the far-infrared and terahertz ranges to create communication devices employing SPPs as carriers of information. In this paper, we consider methods for implementing the multiplex transmission of information along cylindrical conductors using a combination of SPPs with orbital angular momentum and present experimental setups for the experiments on Novosibirsk free electron laser.

INTRODUCTION

It is known that a combination of beams with orbital angular momentum ("vortex " beams) that are propagating in free space can be used to create a multiplex communication channel for data transmission [1,2]. Such a possibility was demonstrated experimentally in the visible [3], radio-frequency [4], and millimeter [5] ranges. One can assume that multiplex plasmon communication systems can be created in a similar way. In this case, the signal will be transmitted over cylindrical conductors using surface plasmon polaritons (SPPs) bearing an orbital angular momentum (OAM). To confirm or refute this assumption, it is necessary to conduct "proof-of-principle " experiments to demonstrate the possibility of generation of vortex plasmons, examine the preservation of their orbital angular momentum during propagation, as well as to develop methods for decoding of signal consisting of a sum of SPPs with different orbital momenta.

In the visible range, the length of path of surface plasmon polaritons, which are also called surface electromagnetic waves, is only tens of microns (see., e.g., [6]). For this reason, it is convenient to start with investigating plasmon communication devices in the most convenient terahertz range, in which the plasmon propagation length is several tens of centimeters on plane surfaces [7] and wires [8]. In this paper, we investigate the first part of this problem: generation of vortex SPPs on cylindrical conductors. We consider three possible methods of their generation, perform parametric analysis of devices intended for experiments in the terahertz range, and describe experimental setups to perform experiments on the Novosibirsk free electron laser.

PLASMONS ON PLANE AND CYLINDRICAL CONDUCTORS

Plasmons have been well studied in the visible and mid-infrared ranges. The measured characteristics of SPPs are in good agreement with calculations performed under the Drude theory, according to which the propagation length of plasmons have to increase as the square of the wavelength. However, measurements of paths of plasmons on plane surfaces in the terahertz ranges turned out to be significantly lower than the calculated ones, both in early [7-9] and modern studies (see, e.g., [10-12]). Radiation losses and ohmic losses exceeding the calculated ones were offered as possible causes.

The interest in terahertz plasmons on cylindrical conductors was renewed due to, among other things, the possibility of lowering the ohmic loss by reducing the proportion of plasmon electromagnetic field in the conductor [13, 14]. Characteristics of plasmons, as shown in theoretical work [15], strongly depend on thin layers of dielectrics deposited on the wire, which makes it possible to use SPPs for diagnostics of coatings. Making a relief on the surface of the wires, e.g., annular grooves, enables control of the dispersion curve of plasmon (in this case, spoof plasmon) and its stronger coupling with the surface, as well as focusing the electromagnetic field on the tips. This possibility was demonstrated by calculations in [16-17]. In [18-20], it was proposed to generate plasmons with orbital angular momentum using cylindrical conductors with subwavelength screw thread. Numerical calculations were performed in the approximation of ideal conductor. Only one attempt was made to experimentally verify the possibility of obtaining vortex plasmons [20], which showed that the absorption resonances of broadband terahertz radiation were at the frequencies predicted by calculations, but no direct measurements of the plasmon field distribution were done. In [21] it was proposed to use a binary helical axicon generating a Bessel beam of the first order for excitation of plasmons at the end face of cylindrical conductor, but no experiments were carried out either.

In our previous works [22-23], we have formed Bessel beams (BBs) of the first and second orders with orbital angular momentum by transforming a Gaussian beam of the Novosibirsk free electron laser [24,25] using binary phase axicons with spiral zone structure [26]. In this paper, we use several versions of optical schemes with axicons to generate vortex plasmons.

GENERATION OF VORTEX PLASMONS USING AXICON AND CYLYNDRICAL GRATING

In the first case (Fig.1a), we use the axicon not as a device to form a Bessel beam, rather as a phase diffraction grating. A beam that passed through a zero-order axicon ($l = 0$) with annular zones forms plane waves conically converging to the axis in the minus first diffraction order. In free space, intersecting, they would form a Bessel beam of zero order. If a reflective cylinder with annular thread is installed on the optical axis, then these waves are diffracted on the grating, reflecting in the planes intersecting the z-axis. If the thread is made reflective in the direction along the surface of the cylinder, then we get a cylindrical equivalent of grating with blazing angle (cylindrical echelette). In the case of spiral axicon (Figs.1b and 1c) the conical wavefront will also rotate. By matching the lattice period with the wavelength, one can direct the diffracted wave along the surface of the grating and forms SPPs on the surface of a replaceable cylinder attached to the grating.

Figures 1a, 1d, and 1e show possible configurations of receiver grating. It is obvious that the plasmon capture efficiency will be the highest for blazing angle gratings that reflect the first order of diffraction along the z-axis. The grating in Fig.1d will be less efficient, but easy to manufacture, and the grating in Fig.1e will enable taking the uncaptured radiation away from the detector.

The mth order diffraction angle of the axicon is (see notation in the figure)

$$\sin\theta_m = \lambda m / p \tag{1}$$

Diffracted beams fall on a coaxial grating at an angle $\theta_i = \pi / 2 - \theta_m$. Then the length of the illuminated part of cylindrical grating is equal to

$$z_2 - z_1 = \frac{R_1 - R_2}{\operatorname{tg}\theta_m} \tag{2}$$

At diffraction of wave falling on a cylindrical grating to the qth order by the angle $\theta_s = \pi / 2$, the condition of generating a plasmon is determined by the law of conservation of momentum:

$$k_z + q\frac{2\pi}{T} = k_s \tag{3}$$

where $k_z = (f / c)\sin\theta_i$ is the longitudinal component of the incident radiation, c is the speed of light, $k_s = \omega / 2\pi v$ is the plasmon wave number on a smooth surface, v is the speed of the plasmon, ω is the radiation angular frequency, and T is the period of the cylindrical grating. In the terahertz range, the speed of the plasmon v practically does not differ from the speed of light in vacuum ($v \approx c$); therefore, condition (3) takes the following form [27]:

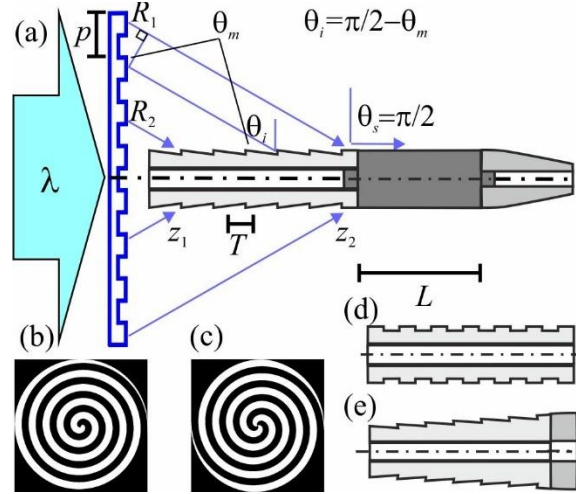$$\frac{\omega(1-\sin\theta_i)}{2\pi} = \frac{q}{T} \tag{4}$$

FIGURE 1. Generation of surface plasmon polaritons using binary phase axicon and cylindrical diffraction grating; (b) and (c) phase functions of binary phase axicons that form Bessel beams of first kind of first and second orders ($l = 1$ and 2), black and white colors corresponding to phase value of 0 and π, respectively; (d) and (e) versions of cylindrical grating relief

Using (1) and (4), we obtain two relations connecting the axicon and grating parameters

$$\begin{cases} p = \dfrac{\lambda m}{\sin \theta_m} = \dfrac{\lambda m}{\cos \theta_i}, \\[2mm] T = \dfrac{q\lambda}{1 - \sin \theta_i}. \end{cases} \tag{5}$$

Since for a binary phase axicon, the diffraction efficiency is the highest for the first diffraction order (~ 41 % in the minus first order), we must put $m = 1$ in expression (5).

For both an axicon and a cylindrical grating, acceptable parameters are obtained with an incidence angle $\theta_i = \theta_m = \pi/4$. The cylindrical grating is phase reflective. When a rectangular-profile grating is used, the reflection maximum will be in the zero order, that is, in the specularly-reflected beam. To obtain the highest diffraction in the $q = 1$ order at the angle $\theta_s = \pi/2$, it is necessary to use a grating with a blazing angle equal to $\pi/8$.

TABLE 1. Parameters of axicons and cylindrical gratings for generating plasmons at various wavelengths.

λ, μm	Silicon axicon (n=3.42)			Cylindrical grating with blazing angle		
	p, μm	h_1, μm	M	T, μm	h_2, μm	N
141	199	29,1	85	480	199	35
47	68	9,9	253	163	68	104
8.5	12	1,76	1416	29	12	586

Parameters of axicons and cylindrical gratings that satisfy Eqs. (5) are given in Table 1, where h_1 and h_2 is the profile depth of the silicon axicon and metal grating, respectively, and M and N are the numbers of periods. Modern technologies enable manufacture of both silicon axicons and cylindrical gratings with the parameters given in the table.

GENERATION OF VORTEX PLASMONS BY DIFFRACTION ON CONDUCTOR END FACE

Generation using Bessel beam

Another way of excitation of vortex plasmons is shown in Fig.2a. A Gaussian beam with a wavelength λ illuminates a silicon axicon with a spiral zone structure. The depth of the relief is

$$h = \lambda / 2(n-1), \tag{6}$$

where n is the refractive index of the axicon material. Passing through the axicon, the beam transforms to the Bessel beam, the electric field of which is described by the expression

$$E(z, r, \varphi) = E_0 J_\ell(\kappa r) \exp[i(k_z z + l\varphi)] \tag{7}$$

$$k = 2\pi / \lambda = \sqrt{k_z^2 + \kappa^2}; \quad \kappa = 2\pi / \lambda \tag{8}$$

where $J_l(\kappa r) = (1/2\pi) \int_0^{2\pi} \exp[\pm i(\kappa r \cos\varphi - l\varphi)]$, r is the radius, and φ is the azimuthal angle. Bessel beams have a "helical" wavefront, consisting of nested helicoidal surfaces, the number of which is equal to the topological charge $l = 0, 1, 2, 3, \ldots$. The spiral grating period p determines the value of the transverse wavenumber $\kappa = 2\pi / p$ of the Bessel beam.
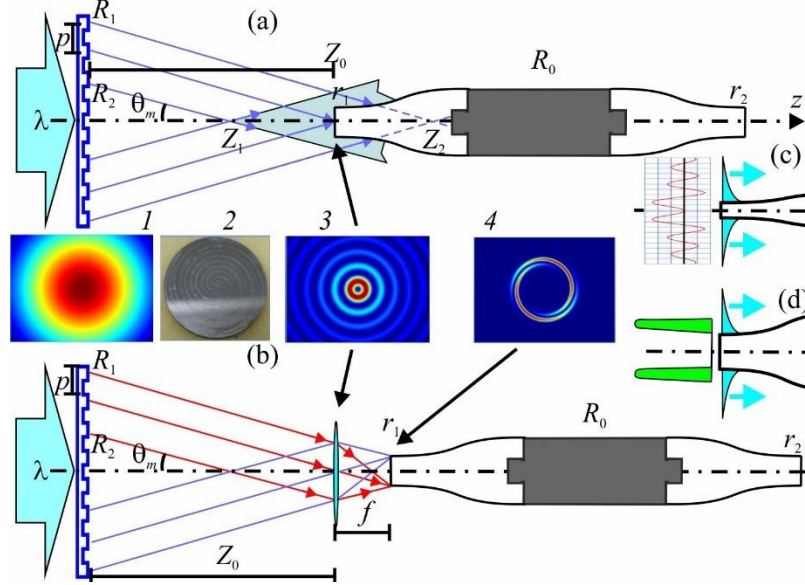

FIGURE 2. Generation of surface plasmon polaritons using binary phase axicon by end-fire coupling technique: (a) generation directly by Bessel beam; (b) generation in focal plane of lens; (c) and (d) amplitudes of second-order BB field and its Fourier image in comparison with distribution of amplitude of SPP field on cylinder. 1 – Gaussian beam, 2 – silicon binary axicon, 3 – Fourier image of BB of second order in focal plane of lens

The ideal BB is a superposition of plane waves conically converging to the optical axis. In a real experiment, the axicon (circular or spiral diffraction grating) is limited in the diameter. Consequently, a quasi-Bessel beam exists only in the zone of intersection of waves bounded by the radii R_1 and R_2, where R_1 is the outer radius of the axicon, and R_2 is the inner radius rays from which still get on the cylindrical grating (Fig.2) . At the distance

$$Z_0 = \frac{R_1 + R_2}{2\,\mathrm{tg}[\arcsin(\lambda / p)]} \xrightarrow{\lambda/p \ll 1} \frac{(R_1 + R_2)p}{2\lambda} \tag{9}$$

where the diffracted waves of the minus first order from the opposite sides of the axicon completely intersect, a BB is formed with the intensity distribution shown in Fig.2a (inset 3). Note that a BB with a constant cross section, which is commonly called non-diffractive, begins to form at the point Z_1 and decays after Z_2 (see details in [23, 28]).

The axicon period is linked with the radius of the maximum intensity of the first ring r_l^{max} by the following relation:

$$p = 2\pi / \kappa = 2\pi r_l^{max} / (\kappa r_l^{max}) \tag{10}$$

where the (κr_l^{max}) values are given in Table 2, and the radius of the coupler (the receiving element of the waveguide) should be matched with the r_l^{max} value:

$$r_c \approx r_c^{\max_l} \tag{11}$$

The coupler in Fig.2 was chosen to be concave-convex to prevent the scattered free wave from getting into the region of propagation of plasmons and on the detectors that measure their intensities.

TABLE 2. Bessel function values $\kappa r^{\max}$ that correspond to first maxima of functions of order l.

l	0	1	2	3	4	5
$(\kappa r_l^{\max})$	0	1,8	3,2	4,3	5,4	6,4

It follows from expressions (10) and (11) that the radius of Bessel beam does not depend on the wavelength for a given topological charge if the axicon period does not change. That is, the same phase axicon will form a BB with the same intensity distribution at any wavelength. However, it is worth noting that the diffraction efficiency is maximal at the calculated wavelength (41 %) and decreases with divergence from it. Nevertheless, for a source with a continuously tunable wavelength, like the Novosibirsk free electron laser, this property of binary axicon is very useful.

If axicons are manufactured with the same period p for all orders l, the radius of rings of the Bessel beams will be proportional to the $(\kappa r_l^{\max})$ values from Table 2, and the distance Z_0 in the paraxial approximation will be inversely proportional to the wavelength. That is, when generating plasmons by the scheme in Fig.2, to ensure high efficiency for each topological charge, it is necessary to change the coupler radius and move the coupler along the axis. Another option is varying the periods of axicons of different orders in inverse proportion to the values given in Table 2. In this case, one coupler can be used to generate vortex plasmons with beams of different orders.

Obviously, the plasmon that arose during BB diffraction on the end face of the coupler will preserve the azimuthal component of the angular momentum of the incident radiation, and its total wave vector will "slip" along the helix on the surface of the cylinder. Note that only a p-polarized wave can excite a plasmon. Therefore, the capture efficiency is maximal if the radiation falling on the axicon is polarized along the normal to the surface (see, e.g., [29-31]). In the case of cylinder, the plasmon exciting radiation must be radially polarized. Such a beam can be obtained, e.g., by interference of two Hermit-Gaussian beams in the Mach-Zehnder interferometer [32] or using a sectional polarizer.

Generation of plasmons using "perfect" vortex beams"

The value of the overlap integral can be made large enough by illuminating the end face of the conductor through an additional lens (Figs.2b and 2d) with a focal length f. In this case, the Fourier image of the Bessel beam is formed in the focal plane of the lens. As known, it is a ring with the radius

$$r_F \approx \lambda f / p \tag{12}$$

which is the same for any l if the axicon period is the same. By changing lenses with different focal lengths, one can easily "fit" the ring radius to the radius of the coupler, thus creating the so-called "perfect" vortex beams. For example, for a wavelength of 141 μm and a period of 3.1 mm, the ring radius at a focal length of 50 mm will be 2.3 mm, and at a wavelength of 47 μm, the same radius will be obtained with a lens with a focal length of 150 mm.

From inset 4 in Fig.2b one can see that the Fourier image of the beam generated by the binary phase axicon is not a continuous ring, as it should be for an ideal beam or in the case of using a multilevel phase element with concentric relief of zones [27]. In our case, the image consists of fragments of nested spirals with alternating phases. This fact is confirmed by both calculations and experiments (see, for example, [23, 37, 38]). This form of ring ruptures in the case of binary spiral axicon is because its phase dependence is a piecewise constant function:

$$\Phi(r,\varphi) = (\pi / 2)\,\mathrm{sgn}(\sin(\kappa r + l\varphi)) \tag{13}$$

At a fixed radius $r = \mathrm{const}$, it has $2l$ zeros at the azimuth angle variation within 2π. An obvious way to obtain a ring Fourier spectrum is to use a kinoform spiral axicon. Nevertheless, such axicon is difficult to manufacture and is designed for one wavelength, whereas the beam quality and properties are much the same as those of ideal Bessel beam, as shown in [28].

Summing up the section, we can say that a binary phase axicon is paradoxically more convenient than a kinoform one and enables easy variation of the experimental conditions.

FITTING OF AXICONS AND COUPLERS PARAMETERS

In the oncoming experiments, one of the most important tasks is to study the conservation of the orbital momentum of vortex plasmon during its propagation along a wire. Given the finite length of plasmon propagation, one of important requirements is the exciting of plasmons with a large twist angle. For this, it is necessary to coordinate the axicon parameters and the diameter of the cylindrical sample and to ensure a plasmon "twist" sufficient to be noticeable throughout plasmon propagation along the conductor. Since the twist angle and the vortex beam radius depend on many parameters of the above devices, it becomes necessary to derive analytical expressions relating them, which are necessary for planning the experiments. Below we present the relevant calculations made for the wavelength range of 8–141 μm, which corresponds to the spectral range in which the generation line of the Novosibirsk free electron laser can be tuned.

Let a Gaussian beam illuminate a spiral phase axicon with a period p, which generates an axisymmetric Bessel beam with OAM and is described by expressions (7) and (8). The trajectory of the Poynting vector is a two-parameter spiral [39]:

$$r = \text{const}, \qquad \phi = \phi_0 + \frac{lz}{r^2 \sqrt{k^2 - \kappa^2}} \tag{14}$$

with the increment

$$\Delta z = \frac{2\pi r^2 \sqrt{k^2 - \kappa^2}}{l}, \tag{15}$$

the value of which grows for peripheral areas as r^2. That is, the inner rings of the Bessel beam rotate much faster than the outer ones. Let us calculate the angle of rotation of the Poynting vector trajectory per unit length of the beam optical axis for the first rings of the Bessel beams created by the binary phase axicons. Differentiating the right-hand expression in (14) and assuming that $\lambda < p$, we obtain

$$\frac{d\phi}{dz} = \frac{\ell}{2\pi r^2 \sqrt{\lambda^{-2} - p^{-2}}} \approx \frac{l\lambda}{2\pi r^2}. \tag{16}$$

The angle of inclination of the Poynting vector trajectory to the z-axis on a cylindrical surface with a radius r is

$$\alpha \approx r \frac{d\phi}{dz} \approx \frac{l\lambda}{2\pi r}. \tag{17}$$

We are interested in the Poynting vector direction in the first maximum of the Bessel function the radius of which is

$$\rho(l, p) = (\kappa r_l) / \kappa = (\kappa r_l) p / 2\pi, \text{ где } \rho(l, p) = r^{\max}. \tag{18}$$

Substituting the values of the argument $(\kappa \rho_l)$ of the Bessel function [40, P.201], we construct the graph shown in Fig.3 (black dots). For further estimates, it is sufficient to approximate it with a linear function $F(l)$, where l is an integer:

$$F(l) \equiv (\kappa \rho_l) \approx (1,244 \pm 0,026)l. \tag{19}$$

Then radius (18) of the first maximum of Bessel beam can be approximated with the expression

$$\rho(\lambda, l) = \frac{F(l)p}{2\pi} \approx 0,20\,\lambda l\,(p/\lambda), \tag{20}$$

and expression (17) will take the form

$$\alpha \approx \frac{l\lambda}{F(l)p} = \frac{0,80}{(p/\lambda)}. \tag{21}$$
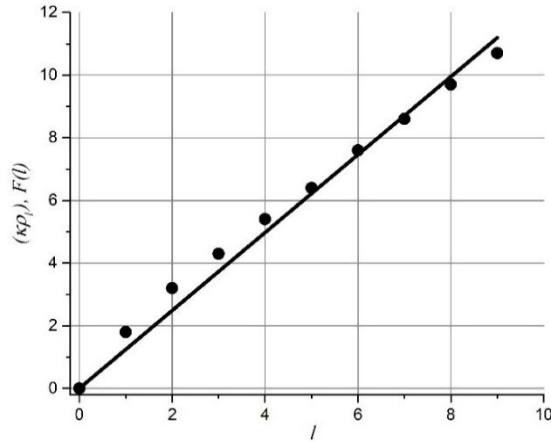
FIGURE 3. Values of $(\kappa\rho_l)$ (dots) and their approximation $F(l)$ (straight line) as a function of modulus of topological charge l (see Table 2)

Thus, for the Poynting vector angle to the optical axis for the first Bessel rings we obtain in our approximation expression (21), independent of the topological charge value and up to a factor coinciding with the classical diffraction formula $\alpha \sim \lambda / p$.

Let us simplify expression (9) to the following form:

$$Z_0 = \frac{R_1 + R_2}{2\,\mathrm{tg}[\arcsin(\lambda / p)]} \approx \langle R \rangle (p / \lambda) .\tag{22}$$

Expressions (20)–(22) make it possible to link the Bessel beam radius, the Poynting vector angle, and the distance at which the beam is formed. All of them depend on the parameter p / λ , and only the radius is also dependent on the wavelength and value of the topological charge l . The dependences of these quantities on the ratio p / λ are shown in the graph presented in Fig.4.
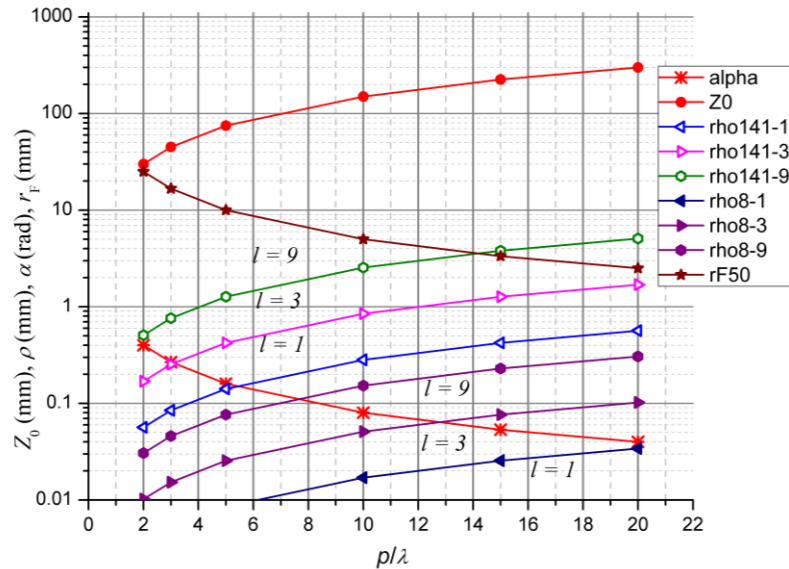

FIGURE 4. Main parameters of Bessel beams formed using spiral phase axicons (see expressions (12), (20)–(22)) vs. ratio of axicon period to radiation wavelength at 141 and 8.5 μm

This graph enables selection of optimal parameters of axicon. The radius of the first ring of the Bessel beam is given

for wavelengths of 8.5 and 141 μm and modules of topological charges $l = 1, 3, 9$. One can see that an acceptable slope of the Poynting vector (of the order of several degrees) is achieved at the ratio p/λ in the range of 4 to 10. In addition, for the terahertz range and large l, the radius of the first Bessel ring lies near one millimeter, while for the mid-IR range it is near 100 μm.

The intersection of the green and brown lines at $p/\lambda = 14$ in the graph is of particular interest. It corresponds to the equality of the radius of the Bessel beam first maximum (at $\lambda = 141$ μm and $l = 9$) to the radius of "perfect" vortex beam obtained from the same beam using a lens with $f = 50$ mm. The radius is 3.5 mm. The angle α is still quite large (≈ 0.053 rad), and the distance at which the BB is formed, $Z_0 \approx 220$ mm, is also convenient for experiments.

EXPERIMENTAL DEVICES

Studies on the generation of vortex plasmons have been started at one of the user stations of the Novosibirsk free electron laser. All three schemes presented above have been realized experimentally. The beams were formed using silicon axicons with holes and without holes (Figs.5a–5c). Various cylindrical elements were used as axisymmetric objects along which plasmons propagated (Fig.5d). To make high-quality surfaces, the samples were prepared on a numerically controlled machine. The manufactured set of bodies of revolution (with dielectric coating, gratings with blazing angle, etc.) makes it easy to modify experimental setups.
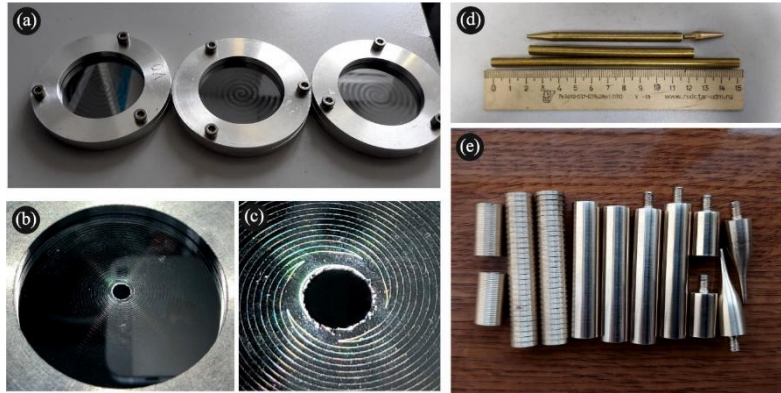

FIGURE 5. (a) Spiral binary phase axicons used for forming Bessel beams with topological charges l =0, ±1, and ±2 at wavelength of 141 μm; (b) and (c) axicon forming Bessel beam with l =±5 at wavelength of 8.5 μm; (d) and (e) snapshots of set of elements for assembling axisymmetric waveguides
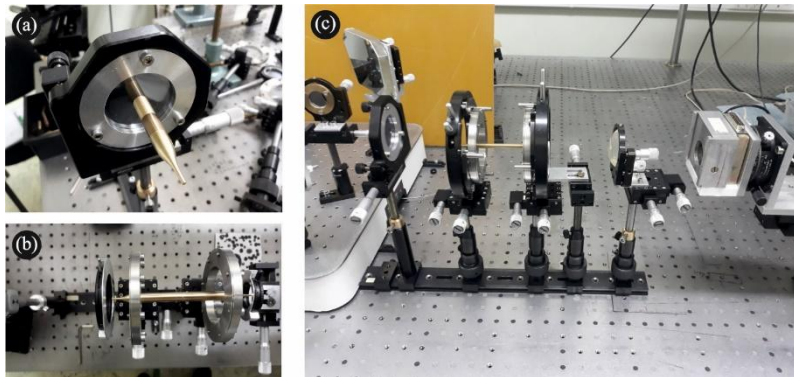

FIGURE 6. a) Binary spiral phase diffraction grating (silicon axicon) with back side exposed to FEL radiation, coupled to cylindrical echelette and axisymmetric brass waveguide; (b) system for studying excitation and transport of SPPs by end-fire coupling technique; (c) the same system with addition of lens for studying Fourier spectrum of radiation diffracted from rear end face of waveguide. Detector: microbolometric array

As an example, Fig.6 presents several assembled structures to explore the capture and transportation of plasmons. Figure 6a shows a system corresponding the scheme shown in Fig.1. On this device, experiments are conducted at a wavelength of 141 μm. The parameters of the axicon and cylindrical brass grating are given in the first line of Table 1. The cylindrical grating was screwed to the axicon using a hole drilled in the axicon, like that in the plate shown in Fig.5b. Smooth axisymmetric waveguides can also be connected to the grating to explore propagation of plasmons, which are expected to occur if the parameters of the exciting wave, axicon, and grating are matched correctly. In the experiments, lattices and cylinders, both uncoated and coated with a ZnS layer 1 μm thick, are used. Our previous experiments have shown that dielectric layers improve the coupling of SPPs with the surface.

Figure 6b presents the optical system corresponding to Fig.2a. In this case, plasmons are excited by the end-fire coupling technique at diffraction of Bessel beams on the end face of metal waveguide. The waveguides, consisting of screwed-up parts, are supported by polypropylene films stretched over ring supports; the thickness of the films is much less than the wavelength and they have a whole on the axis. It has been shown in [37] that SPPs passing through thin films obey the same laws as a free wave does. Figure 6c shows another embodiment of the end-fire coupling technique, when the Fourier spectrum of the radiation from the end of the waveguide is recorded by a microbolometric detector array with the use of *f-f* focusing system. Recording of the Fourier spectrum enables derivation of the angular spectrum of radiation. This feature will be useful for studying the degree of twist of radiation diffracted from the exit end face. In various versions of experimental setups, either a high-sensitivity microbolometric detector array with a small matrix size (16.32x12.24 mm) or a less sensitive Pyrocam IV with a matrix size of 25.6x25.6 mm is used as the image recorder in both the terahertz and mid-infrared ranges.

The NovoFEL shutdown because of the pandemic suspended the studies at the initial stage. We hope to present the first physical results soon after the resumption of the installation operation.

SUMMARY

Two methods for generating ring surface plasmon polaritons (SPPs) using high-order Bessel beams are shown. In the first method, free radiation is transformed into an SPP using a binary phase axial grating which illuminaties a cylindrical diffraction grating connected to a cylindrical waveguide. The second method uses the diffractive coupling of a Bessel beam to an axisymmetric conductor. In this case, as an option, before the capture, a lens can first transform the beam to form an annular vortex beam at its focus. After passage through the waveguide, the mode composition of the beam is decoded, for example, using diffractive optical elements, and each communication channel has an individual detector. Devices that implement these methods has been demonstrated.

ACKNOWLEDGMENTS

REFERENCES

1. A.E. Willner, H. Huang, Y. Yan, Y. Ren, N. Ahmed, G. Xie, C. Bao, L. Li, Y. Cao, Z. Zhao, J. Wang, A.E., Advances in Optics and Photonics **7**(1), 66-106 (2015).
2. А. А. Алмазов, С.Н. Хонина, В. В. Котляр, Оптический журнал **72**(5), 45-54 (2005).
3. M. Krenn, R. Fickler, M. Fink, J. Handsteiner, M. Malik, T. Scheidl, R. Ursin, A. Zeilinger, New Journal of Physics, **16**(11), 113028 (2014).
4. F. Tamburini, E. Mari, A. Sponselli, B. Thidé, A. Bianchini, F. Romanato, New Journal of Physics **14**(3), 033001 (2012).
5. Y. Yan, G. Xie, M. P. Lavery, H. Huang, N. Ahmed, C. Bao, Y. Ren, Y. Cao, L. Li, Z. Zhao, A. F. Molisch, Nature Communications **5**(1), 1-90 (2014).
6. X. Zhang, Q. Xu, L. Xia, Y. Li, J. Gu, Z. Tian, C. Ouyang, J. Han, W. Zhang, Advanced Photonics **2**(1), 014001 (2020).
7. D. L. Begley, R. W. Alexander, C. A. Ward, R. Miller, R. J. Bell, Surface science **81**(1):245-51 (1979).
8. E. S. Koteles and W. H. McNeill, Int. J. Infrared, Millimeter, Terahertz Waves **2**, 361–371 (1981).
9. Z. Schlesinger, B. C. Webb, and A. J. Sievers, Solid State Commun. **39**, 1035–1039 (1981).

10. T. I. Jeon, D. Grischkowsky, Applied physics letters **88**(6), 061113 (2006).
11. M. Nazarov, F. Garet, D. Armand, A. Shkurinov, J.L. Coutaz, Comptes Rendus Physique **9**(2), 232-47 (2008).
12. B. A. Knyazev, V. V. Gerasimov, A. K. Nikitin, I. A. Azarov, Y. Y. Choporova, JOSA B **36**(6), 1684-9 (2019).
13. K. Wang, D. M. Mittleman, Nature **432**(7015), 376 (2004).
14. K. Wang, D. M. Mittleman, JOSA B **22**(9), 2001-8 (2005).
15. N. C. Van der Valk, P. C. Planken, Applied Physics Letters **87**(7), 071106 (2005).
16. S. A. Maier, S. R. Andrews, L. Martin-Moreno, F. J. Garcia-Vidal, Physical Review Letters **97**(17), 176805 (2006).
17. A. I. Fernandez-Dominguez, L. Martin-Moreno, F. J. Garcia-Vidal, S. R. Andrews, S. A. Maier, IEEE Journal of Selected Topics in Quantum Electronics **14**(6), 1515-21 (2008).
18. F. Rüting, A. I. Fernández-Domínguez, Martín-Moreno L, García-Vidal FJ., Physical Review B **86**(7), 075437 (2012).
19. H. Z. Yao, S. Zhong, IEEE Photonics Journal **7**(6), 1-7 (2015).
20. A. I. Fernández-Domínguez, C. R. Williams, F. J. García-Vidal, L. Martín-Moreno, S. R. Andrews, S. A. Maier, Applied Physics Letters **93**(14), 141109 (2008).
21. A. Edelmann, S. Helfert, J. Jahns, Complex Light and Optical Forces VIII **8999**, 899913 (2014).
22. B. A. Knyazev, Y. Y. Choporova, M. S. Mitkov, V. S. Pavelyev, B. O. Volodkin, Phys. Rev. Lett. **115**(16), 163901 (2015).
23. Y. Y. Choporova, B. A. Knyazev, G. N. Kulipanov, V. S. Pavelyev, M. A. Scheglov, N. A. Vinokurov, B. O. Volodkin, V. N. Zhabin. Phys. Rev. A **96**(2), 023846 (2017).
24. O. A. Shevchenko, V. S. Arbuzov, N. A. Vinokurov, P. D. Vobly, V. N. Volkov, Y. V. Getmanov, Y. I. Gorbachev, I. V. Davidyuk, O. I. Deychuly, E. N. Dementyev, B. A. Dovzhenko, Physics Procedia **84**,13-18 (2016).
25. B. A. Knyazev, I. A. Azarov, E. N. Chesnokov, Y. Y. Choporova, V. V. Gerasimov, Y. I. Gorbachev, Y. V. Getmanov, B. G. Goldenberg, O. E. Kameshkov, P. V. Koshlyakov, I. A. Kotelnikov, EPJ Web of Conferences **195**, 00002 (2018).
26. N. E. Andreev, S. S. Bychkov, V. V. Kotlyar, L. Y. Margolin, L. N. Pyatnitskii, and P. G. Serafimovich, Quantum Electron **26**, 126-130 (1996).
27. V. Arrizon, D. Sanchez-de-La-Llave, U. Ruiz, G. Mendez, Optics letters **34**, 1456-1458 (2009).
28. B. A. Knyazev, V. G. Serbo, Phys. Usp. **61**(5), 449 - 479 (2018).
29. G. N. Zhizhin, M. A. Moskaleva, E. V. Shomina, and V. A. Yakovlev, Surface Polaritons. Electromagnetic Waves at Surfaces and Interfaces 93-144(1982).
30. F.V. Kuzmin, B.A. Knyazev, Vestnik NSU **2**(1), 109-122 (2007).
31. E.S. Kozlova and V.V. Kotlyar, Computer optics **40**(5), 629-634 (2016).
32. Q. Zhan, Advances in Optics and Photonics **1**, 1-57 (2009).
33. S. N. Khonina, A. P. Porfirev, Applied Physics B **124**(9), 191 (2018).
34. S. Syubaev, A. Zhizhchenko, O. Vitrik, A. Porfirev, S. Fomchenkov, S. Khonina, S. Kudryashov, A. Kuchmizhak, Applied Surface Science **470**, 526–534 (2019).
35. M. V. Berry, K. T. McDonald, Journal of Optics A: Pure and Applied Optics **10**(3), 035005 (2008).
36. F. Lösch, F. Emde, E. Jahnke, *Tables of higher functions (*McGraw-Hill: Book, New York, 1960), p. 201.
37. V. V. Gerasimov, A. K. Nikitin, A. G. Lemzyakov, I. A. Azarov, I. A. Milekhin, B. A. Knyazev, E. A. Bezus, E. A. Kadomina, L. L. Doskolovich, Journal of Optical Society of America B, **37**(5), 1461-1467 (2020).